CHEMISTRY OF MATERIALS

Article

pubs.acs.org/cm

Core–Shell Layered Double Hydroxide Microspheres with Tunable Interior Architecture for Supercapacitors

Mingfei Shao, Fanyu Ning, Yufei Zhao, Jingwen Zhao, Min Wei,* David G. Evans, and Xue Duan

State Key Laboratory of Chemical Resource Engineering Beijing University of Chemical Technology Beijing 100029 (P. R. China)

Supporting Information

ABSTRACT: Core–shell layered double hydroxide microspheres with tunable interior architecture have been synthesized by a facile and cost-effective *in situ* growth method. The SEM and TEM images revealed that the obtained microspheres display a three-dimensional architecture with core–shell, yolk–shell, and hollow interior structure respectively, with continuous changes in specific surface area and pore-size distribution. Moreover, the hollow NiAl-LDH microspheres exhibit excellent pseudocapacitance performance, including high specific capacitance and rate capability, good charge/discharge stability and long-term cycling life, owing to the greatly improved faradaic redox reaction and mass transfer. Therefore, this work provides a promising approach for the design and synthesis of structure tunable materials with largely enhanced supercapacitor behavior, which can be potentially applied in energy storage/conversion devices.

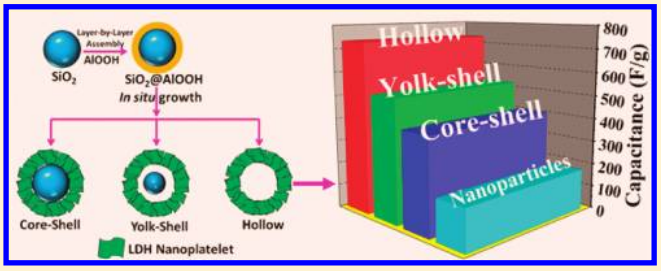

KEYWORDS: *layered double hydroxides, core–shell microspheres, tunable architecture, supercapacitors*

INTRODUCTION

Ever worsening energy depletion and global warming have stimulated intense research on energy storage and conversion from alternative energy sources. Supercapacitors, also known as electrochemical capacitors (ECs) or ultracapacitors, are considered as a promising candidate for next-generation power devices because of their advantages of fast charging and discharging, high power delivery, and excellent cycling lifespan in comparison with conventional batteries and dielectric capacitors.[1−5] On the basis of the charge storage mechanisms, electrochemical supercapacitors are broadly divided into electrical double layer capacitors (EDLCs) and pseudocapacitors. In particular, pseudocapacitors entail reversible faradic redox reactions on the surface of an electro-active material for charge storage, which have a higher specific capacitance value of 10−100 times that of EDLCs.[6,7] Metal (Ru, Co, Ni, etc.) oxides and hydroxides are typical pseudocapacitive active species due to their relatively higher capacitance and fast redox kinetics.[8−11] However, these materials often suffer from a low power performance and cycle life because redox kinetics is limited by the rate of mass diffusion and electron transfer. Some efforts have been made to improve the performance of pseudocapacitive materials by creating nanostructures, such as core/shell nanowires or microfibers,[12,13] nanowall films,[14,15] and conductive graphene or polymers supported metal oxides/hydroxides hybrid materials.[16−18] Despite the progress, a huge challenge still remains to achieve high specific capacitor and long-lasting supercapacitors simultaneously.

To solve this problem, three strategies can be taken into account. First, electroactive materials with multiple redox states are essential for the enhancement of pseudocapacitance for a supercapacitor. Second, the specific surface area of the electrode materials needs to be as high as possible to accommodate a large amount of superficial electroactive species to participate in faradaic redox reactions. Third, suitable mesopores (especially 2−5 nm) of the electrode materials are also critical to ease the mass transfer of electrolytes for fast redox reactions. Layered double hydroxides (LDHs) are a class of 2D structure anionic clays, which have been widely used in the fields of catalysis,[19−21] visible-light photocatalysis,[22] biology,[23] magnetics,[24] optical materials,[25,26] and electrodes for electrochemical sensors and alkaline secondary batteries.[27−29] LDH/carbon hybrid materials have been reported as promising electrode materials for supercapacitors owing to their low cost, high redox activity, and environmentally friendly nature.[30] However, the relatively poor cycling life and complicated fabrication process limit their practical applications. A key challenge for LDHs in the application of supercapacitors is to build up a well-defined micro/nanostructures with high surface area and mesoporous pore-size distribution,[31] in which all the electroactive species participate in faradic redox reactions and a fast mass and electron transfer is guaranteed.

Herein, we demonstrate the design and fabrication of NiAl-LDH microspheres with tunable interior architecture from core–shell to hollow structure *via* a layer-by-layer (LBL) deposition followed by an *in situ* growth technique, and the

Received: December 22, 2011
Revised: February 27, 2012
Published: March 5, 2012

hollow microspheres show excellent pseudocapacitance properties. The LDH shell immobilized on a SiO_2 core with core–shell, yolk–shell, and hollow structure was obtained by controlling the preparation conditions. Moreover, mesopores appear gradually with the shrinking of the silica core, which also facilitates to the improvement of the pseudocapacitance property. The hollow NiAl-LDH microspheres with the highest surface area and a mesopore distribution (3–5 nm) give a maximum specific capacitance of 735 F/g, much larger than that of core–shell (406 F/g) and yolk–shell (524 F/g) microspheres (at 2 A/g; based on pristine LDH). In addition, the hollow microspheres show good cycle performance (the capacitance increases 16.5% after 1000 cycles at a high charge/discharge current density of 8 A/g) and remarkable rate capability (75% capacitance was retained at a large current density of 25 A/g). This work provides a facile approach for the fabrication of hierarchical LDH materials by tuning interior architecture, which can be potentially used in energy storage and conversion devices.

EXPERIMENTAL SECTION

Synthesis. The monodisperse silica spheres were prepared by hydrolysis of tetraethyl orthosilicate (TEOS) in an alcohol medium in the presence of water and ammonia by a modified procedure of the well-known Stöber method.[32] The AlOOH primer sol was prepared according to the method reported by our group,[33] and the SiO_2/AlOOH microspheres were then prepared by a layer-by-layer method. Typically, the prepared silica spheres were dispersed in the AlOOH primer sol for 2 h with vigorous agitation, followed by withdrawing *via* centrifugation, and then washing thoroughly with ethanol. The resulting SiO_2/AlOOH microspheres were dried in air for 30 min. The whole process (dispersion, withdrawing, drying) was repeated 10 times. An *in situ* crystallization of a NiAl-LDH nanoplatelet shell on the surface of SiO_2/AlOOH microspheres was carried out. The SiO_2/AlOOH microspheres (0.1 g) were placed in a 70 mL deionized water containing 0.01 mol of $Ni(NO_3)_2{\cdot}6H_2O$ and various concentration of urea (2.5×10^{-4}, 1.2×10^{-3} and 3.2×10^{-3} mol, respectively) in an autoclave at 100 °C for 48 h. Finally, the resulting LDH microspheres were separated by centrifugation, rinsed with ethanol and dried at room temperature. The synthesis details for MgAl-LDH microspheres with tunable interior structure and the comparison sample NiAl-LDH nanoparticles are described in the Supporting Information.

Material Characterization. Powder X-ray diffraction patterns of the microsphere samples were collected on a Shimadzu XRD-6000 diffractometer using a Cu Kα source, with a scan step of 0.02° and a scan range between 3° and 80°. The morphology of the microspheres was investigated using a scanning electron microscopy (SEM) instrument (Zeiss SUPRA 55) with an accelerating voltage of 20 kV, combined with energy dispersive X-ray (EDX) spectroscopy. Transmission electron microscopy (TEM) images were recorded with Philips Tecnai 20 and JEOL JEM-2010 HR-TEM. The accelerating voltage was 200 kV in each case. The specific surface area determination, pore volume, and size analysis were performed by Brunauer–Emmett–Teller (BET) and Barrett–Joyner–Halenda (BJH) methods, respectively, using a Quantachrome Autosorb-1C-VP analyzer. Prior to the measurements, the samples were degassed at 100 °C for 6 h.

Electrochemical Characterization. Electrochemical measurements were performed on an electrochemical workstation (CHI 660C, CH Instruments Inc., Shanghai) using a three-electrode mode in 1 M KOH aqueous solution within the potential window from −0.1 to 0.5 V. The working electrode (1 cm × 1 cm) was prepared by mixing LDH microspheres (80 wt %) as active material with acetylene black (15 wt %) and polyvinylidene fluoride (5 wt %). The slurry was coated on a nickel foam substrate and dried at 60 °C for 30 min. The as-formed electrode was then pressed at 10 MPa and further dried at 100 °C for 6 h. The reference and counter electrode were Ag/AgCl and platinum electrode, respectively. EIS measurements were performed by applying an AC voltage with 5 mV amplitude in a frequency range from 0.01 to 100 kHz. Specific capacitance was calculated by using eq 1, where I is the constant discharge current; t is the discharging time; ΔV is the voltage drop upon discharging; and m is the mass of pristine NiAl-LDH.

$$C = \frac{It}{\Delta V m} \tag{1}$$

RESULTS AND DISCUSSION

The LDH microspheres with tunable interior architecture from core–shell to hollow structure are fabricated by coating ultrathin AlOOH film to silica microspheres, followed by *in situ* growth technique. The general fabrication protocol is illustrated in Scheme 1.

Scheme 1. Preparation of LDH Microspheres with Tunable Interior Architecture from Core–Shell to Hollow Structure

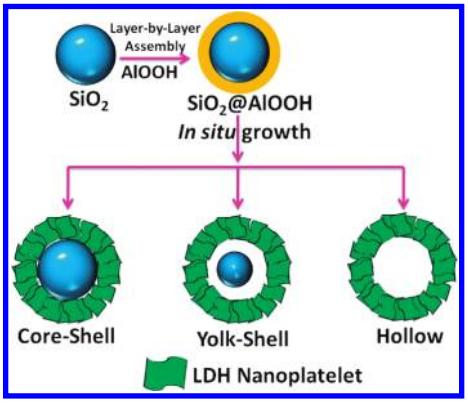

First, monodisperse silica microspheres (0.34 μm; Figure S1, Supporting Information) were prepared by a modified procedure of the well-known Stöber method.[32] The obtained silica spheres were then subjected to AlOOH primer sol for 2 h, followed by withdrawing the microspheres by centrifugation and then washing thoroughly with ethanol. The whole process was repeated 10 times. After being coated with thin AlOOH film (12 nm, Figure 1A, E), the SiO_2/AlOOH core–shell microspheres transformed to SiO_2/LDH microspheres by reaction with an alkaline solution containing Ni^{2+} ions. Parts B, C, and D of Figure 1 display typical SEM images of NiAl-LDH microspheres obtained with different alkaline concentration, illustrating a well-dispersed and near-spherical morphology with particle size of ~0.63 μm. The as-synthesized flowerlike microspheres are composed of numerous nanoflakes (~0.15 μm in width and ~18 nm in thickness) intercrossed with each other grafted to the substrate. TEM images of the resulting LDH microspheres prepared with different alkaline concentration (Figure 1F, G, and H) reveal core–shell, yolk–shell, and hollow spherical structures, respectively. It can be seen that the inner diameter of hollow LDH microspheres (330–340 nm) is close to the particles size of silica precursor (~340 nm). The high resolution TEM (HR-TEM) image shows lattice fringes corresponding to an interplanar distance of ~0.24 nm that can be attributed to the (012) plane of a NiAl-LDH phase (Figure S2, Supporting Information).

Figure 2 shows the XRD patterns of SiO_2, SiO_2/AlOOH, SiO_2/NiAl-LDH microspheres with various interior architecture respectively. Curve a presents a reflection characteristic of amorphous SiO_2; after coating with a AlOOH layer, the

dx.doi.org/10.1021/cm203831p | *Chem. Mater.* 2012, 24, 1192–1197

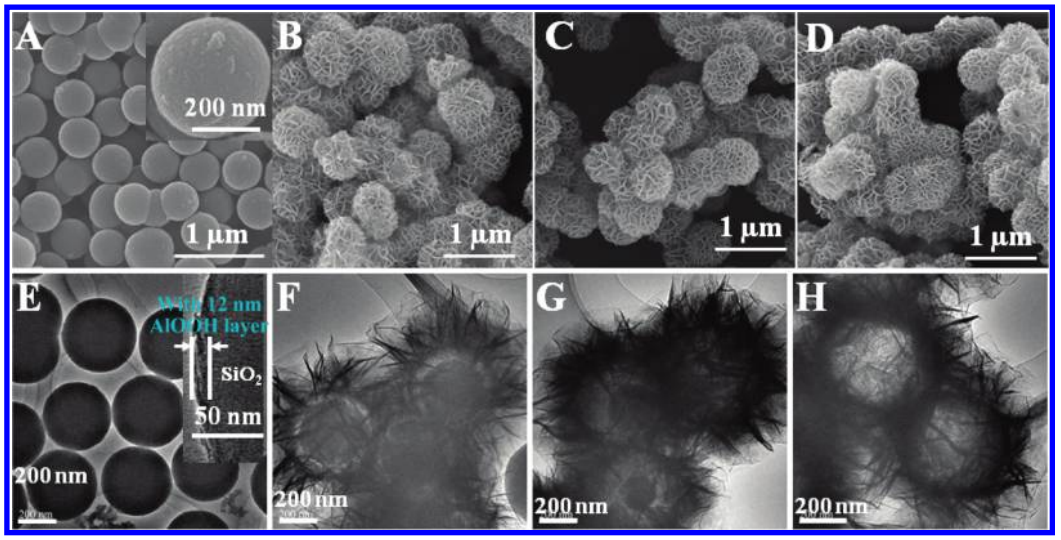

Figure 1. TEM and SEM images of (A, E) SiO_2/AlOOH microspheres; (B, F) SiO_2/NiAl-LDH core–shell microspheres; (C, G) SiO_2/NiAl-LDH yolk–shell microspheres; (D, H) NiAl-LDH hollow microsphere.

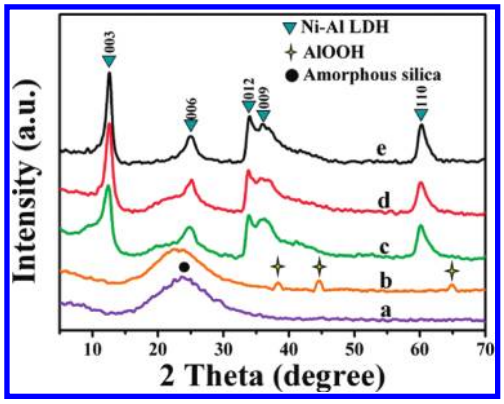

Figure 2. XRD patterns of (a) SiO_2, (b) SiO_2/AlOOH, (c) SiO_2/LDH core–shell, (d) SiO_2/LDH yolk–shell, and (e) hollow LDH microsphere.

reflections due to the AlOOH phase were observed in addition to SiO_2. The XRD patterns of the resulting LDH microspheres (curves c, d, e) after the *in situ* growth process exhibit a series of (003), (006), (012), and (110) reflections, which can be indexed to an LDH phase, indicating the phase transformation from AlOOH to LDH material. It should be noted that the reflection intensity of amorphous SiO_2 gradually decreases from curve c to curve e, revealing the gradual disappearance of the core along with the increase of alkaline concentration in the growth process of LDH shell.

The EDX spectrometry (Figure S3, Supporting Information) shows the presence of nickel and aluminum for the three samples. However, the content of silicon decreases remarkably from core–shell to hollow structure, which is in good agreement with the results of TEM (Figure 1), XRD (Figure 2), and elemental analysis (Table S1, Supporting Information). The results demonstrate that the interior architecture of the LDH microspheres can be simply tuned by changing the preparation parameter. The dissolution of SiO_2 core occurs simultaneously accompanied with the phase transformation of AlOOH to LDH material; a high concentration of alkaline leads to hollow structure of LDH microspheres. In addition, this method can be readily extended to the fabrication of other LDH microspheres by changing the divalent metal precursor. The example of MgAl-LDH microspheres with tunable interior structure is shown in Figure S4 in the Supporting Information, demonstrating the feasibility and generality of this approach in controlling the morphology of LDH materials.

The surface area and pore-size distribution are two key factors for the electroactive materials in supercapacitor applications. Therefore, the core–shell, yolk–shell, and hollow samples were investigated for their surface area and porosity property by N_2-adsorption/desorption measurement (Figure 3). In all the cases, typical IV isotherms with H3-type hysteresis

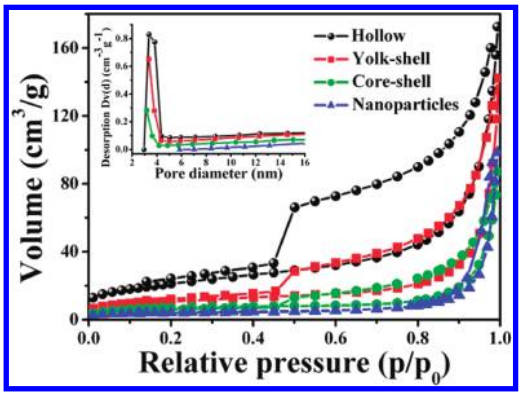

Figure 3. N_2-sorption isotherms and pore size distribution (inset) of SiO_2/LDH core–shell, yolk–shell, and hollow LDH microspheres.

loops (P/P_0 > 0.4) are observed, indicating the presence of mesopores.[34] This type of hysteresis loops does not exhibit any limiting adsorption at high P/P_0 region, which is commonly attributed to particle aggregates with slit-shaped pores.[35] However, the pore size of the LDH microspheres increases markedly along with the shrinking of silica core (Figure 3, inset). Typically, the hollow microspheres give a complete mesopore distribution in the size 3–5 nm. It was reported that the pore-size distribution within 2–5 nm is optimal for the behavior of supercapacitors,[36,37] which will be further discussed in the next section. In contrast, the LDH nanoparticles sample (Figure S5, Supporting Information), which was studied for comparison shows no mesopores in the range 2–5 nm (Figure 3, inset, blue line). Moreover, the maximum specific surface

dx.doi.org/10.1021/cm203831p | *Chem. Mater.* 2012, 24, 1192–1197

area is presented in the sample of hollow LDH microspheres (124.7 m^2/g), much larger than that of yolk–shell (68.5 m^2/g), core–shell (42.3 m^2/g), and LDH nanoparticles (13.8 m^2/g).

The electrochemistry properties of the LDH microspheres were further evaluated. Figure 4A shows the cyclic voltammo-

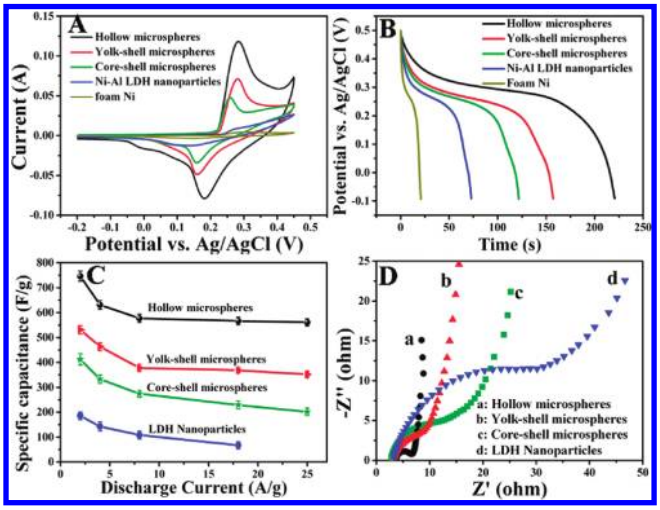

Figure 4. (A) Cyclic voltammograms (CVs) curves; (B) galvanostatic (GV) discharge curves; (C) current density dependence of the specific capacitance; (D) Nyquist plots of the EIS for the hollow, yolk–shell, core–shell LDH microspheres, and LDH nanoparticles (reference sample).

grams (CVs) of different electrodes in 1 M KOH solution at a scan rate of 30 mV s^{-1}. Each CV curve of the LDH microspheres consists of a pair of redox peaks, corresponding to the reversible redox of Ni^{2+}/Ni^{3+} associated with OH^-.[38] A much larger redox current as well as lower ΔEp were obtained for the hollow spheres than the other two samples, and the ratio between the anodic and cathodic peak current is ~1.0. This indicates a more reversible faradic redox reaction for the hollow structure, which plays a key role in contributing to the pseudocapacitance.

The specific capacitance values for the hollow, yolk–shell, core–shell microspheres and LDH nanoparticles are calculated to be 703, 416, 360, and 117 F/g (based on pristine LDH), respectively, according to the CV. Figure 4B shows the galvanostatic (GV) discharge characteristics of different LDH microspheres within a potential range −0.1 to 0.5 V, in which the nonlinear charge/discharge curves verify the pseudocapacitance nature.[39] This is consistent with the result of CVs (Figure 4A). The corresponding specific capacitance is 735, 524, 406, and 177 F/g at a current density of 2 A/g for the hollow, yolk–shell, core–shell microspheres, and LDH nanoparticles, respectively, which further confirms the highest specific capacitance of the hollow sample. Rate capability is a key factor for evaluating the power applications of supercapacitors. The specific capacitances of the four samples derived from the discharging curves (Figure S6, Supporting Information) at different charge/discharge rates (current densities) are shown in Figure 4C. At a high current density of 25 A/g, the specific capacitance retained 75% (from 735 F/g to 548 F/g) for the hollow spheres, whereas the yolk–shell kept 65.5%, the kept core–shell 48.1%, and LDH nanoparticles almost lost all the specific capacitance completely. In addition, the capacitance per surface area is also shown in Figure S7 in the Supporting Information. The hollow LDH microspheres still demonstrate higher capacitance (~0.73 F/cm^2) compared with yolk–shell (~0.52 F/cm^2), core–shell (~0.41 F/cm^2), and LDH nanoparticles (~0.17 F/cm^2) at a current density of 2 mA/cm^2. The enhancement of specific capacitance and superior rate capability of the hollow LDH microspheres are mainly attributed to the specific nanostructure with large surface area, which provides effective diffusion channels for the electrolyte ions (OH^-). In particular, the abundant mesopores in the structure can act as an "ion reservoir", which guarantees a steady supply of OH^- ions as well as high current density of the faradic reaction for energy storage.

The enhanced electrochemical performance of the hollow microspheres was further confirmed by the electrochemical impedance spectroscopy (EIS) measurements. Figure 4D shows the Nyquist plots of the EIS spectra for hollow (curve a), yolk–shell (curve b), core–shell (curve c), and LDH nanoparticles (curve d), respectively. The semicircle diameter of EIS equals the electron transfer resistance (R_{et}), which controls the electron transfer kinetics of the redox Ni^{2+}/Ni^{3+} couple at the electrode interface.[40,41] The semicircle-like shape for the EIS spectra of these samples was observed with the sequence order of R_{et}: hollow< yolk–shell < core–shell < LDH nanoparticles. The results are in high agreement with their CV and GV behavior, which clearly demonstrates that the hollow structure possesses lower resistance and thus allows for much faster electron transfer. For the Ni-based hydroxide supercapacitor system, the redox process involves the reversible uptake and release of OH^- from solution associated with electron transfer from/to the current collector.[42,43] The lower resistance of the hollow LDH microspheres indicates a faster electron transfer between the active material and the charge collector. This is probably due to the higher specific surface area of the hollow microspheres compared with other LDH samples, which facilitates the effective exposure of active sites.

Cycling capability or cycling life is an important requirement for supercapacitor applications. The cycling life tests over 1000 cycles for these LDH microspheres at a current density of 8 A/g were carried out using galvanostatic charge/discharge technique in the potential window −0.1 to 0.5 V (Figure 5). It is noted that the LDH nanoparticles show the worst cycling stability (37.3% loss), possibly resulting from the compact particles, which are detrimental to electrolyte transport and active site accessibility during the cycling process.[39] However, the yolk–shell and core–shell LDH microspheres display good

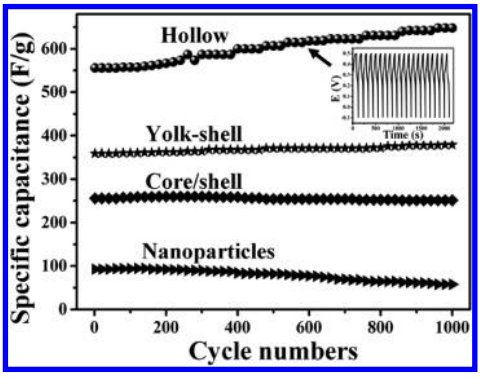

Figure 5. Cycling performance of the hollow, yolk–shell, core–shell structure, and LDH nanoparticles (1000 cycles). The inset shows the charge/discharge curves of the last 20 cycles for the hollow LDH microspheres.

dx.doi.org/10.1021/cm203831p | *Chem. Mater.* 2012, 24, 1192–1197

charge/discharge stability with 5.6% increase and 1.8% loss, respectively. Inspiringly, the specific capacitance of the hollow LDH microspheres increases by 16.5% after 1000 cycles (from 556 to 648 F/g). The long-term electrochemistry stability can be further demonstrated by the very stable charge−discharge curves shown in the inset of Figure 5 (the last 20 cycles). The enhancement of capacitance can be attributed to the increasing active species exposed to the electrolyte upon repetitive charge/discharge cycling.[30] Moreover, the large surface area and optimal pore-size of the hollow microspheres guarantee the high specific capacitance and excellent cycle stability.

■ CONCLUSIONS

In conclusion, LDH microspheres with tunable interior architecture were synthesized by a facile and cost-effective *in situ* growth approach. The obtained microspheres exhibit a three-dimensional architecture with core−shell, yolk−shell and hollow interior structure, respectively. The hollow LDH microspheres exhibit excellent pseudocapacitance performance, including high specific capacitance and rate capability, good charge/discharge stability and long-term cycling life, superior to the yolk−shell and core−shell structure. This can be ascribed to the specific 3D architecture with enhanced surface area and suitable mesopore distribution, which improves the faradic redox reaction and benefits the mass transfer of electrolytes. Therefore, the hollow NiAl-LDH microspheres meet the requirements of both high specific capacitance and long cycle lifetime, which have promising application in future energy storage/conversion devices. It is expected that the approach for tuning the interior structure of LDH microspheres can be extended to other oxide or hydroxide materials for the purpose of obtaining largely enhanced physiochemical property.

■ ASSOCIATED CONTENT

Ⓢ Supporting Information

The experimental details of the preparation of the MgAl-LDH microspheres and NiAl-LDH nanoparticles; SEM image of the prepared silica microspheres; HR-TEM of the NiAl-LDH nanoparticles; SEM and TEM images of the MgAl-LDH microspheres; galvanostatic discharge curves at various discharge current densities for the NiAl-LDH microspheres and nanoparticles. This material is available free of charge via the Internet at http://pubs.acs.org.

■ AUTHOR INFORMATION

Corresponding Author

*E-mail: weimin@mail.buct.edu.cn.

Notes

The authors declare no competing financial interest.

■ ACKNOWLEDGMENTS

This work was supported by the 973 Program (Grant No. 2011CBA00504), the National Natural Science Foundation of China, the 111 Project (Grant No. B07004) and the Collaboration Project from the Beijing Education Committee.

■ REFERENCES

(1) Winter, M.; Brodd, R. J. *Chem. Rev.* **2004**, *104*, 4245.
(2) Miller, J. R.; Simon, P. *Science* **2008**, *321*, 651.
(3) Simon, P.; Gogotsi, Y. *Nat. Mater.* **2008**, *7*, 845.
(4) Wei, T. Y.; Chen, C. H.; Chien, H. C.; Lu, S. Y.; Hu, C. C. *Adv. Mater.* **2010**, *22*, 347.
(5) Prasad, K. R.; Koga, K.; Miura, N. *Chem. Mater.* **2004**, *16*, 1845.
(6) Jayalakshmi, M.; Balasubramanian, K. *Int. J. Electrochem. Sci.* **2008**, *3*, 1196.
(7) Conway, B. E.; Birss, V.; Wojtowicz, J. *J. Power Sources* **1997**, *66*, 1.
(8) Soudan, P.; Gaudet, J.; Guay, D.; Bélanger, D.; Schulz, R. *Chem. Mater.* **2002**, *14*, 1210.
(9) Xu, M. W.; Kong, L. B.; Zhou, W. J.; Li, H. L. *J. Phys. Chem. C* **2007**, *111*, 19141.
(10) Yuan, C. Z.; Zhang, X. G.; Su, L. H.; Gao, B.; Shen, L. F. *J. Mater. Chem.* **2009**, *19*, 5772.
(11) Wei, T. Y.; Chen, C. H.; Chang, K. H.; Lu, S. Y.; Hu, C. C. *Chem. Mater.* **2009**, *21*, 3228.
(12) Bao, L. H.; Zang, J. F.; Li, X. D. *Nano Lett.* **2011**, *11*, 1215.
(13) Bae, J.; Song, M. K.; Park, Y. J.; Kim, J. M.; Liu, M.; Wang, Z. L. *Angew. Chem., Int. Ed.* **2011**, *50*, 1.
(14) Liu, J.; Cheng, C.; Zhou, W.; Lia, H.; Fan, H. J. *Chem. Commun.* **2011**, *47*, 3436.
(15) Wu, J. B.; Lin, Y.; Xia, X. H.; Xu, J. Y.; Shi, Q. Y. *Electrochim. Acta* **2011**, *56*, 7163.
(16) Wang, H. L.; Casalongue, H. S.; Liang, Y.; Dai, H. J. *J. Am. Chem. Soc.* **2010**, *132*, 7472.
(17) Zhang, X. J.; Shi, W. H.; Zhu, J. X.; Kharistal, D. J.; Zhao, W. Y.; Lalia, B. S.; Hng, H. H.; Yan, Q. Y. *ACS Nano* **2011**, *5*, 2013.
(18) Du, F.; Yu, D.; Dai, L.; Ganguli, S.; Varshney, V.; Roy, A. K. *Chem. Mater.* **2011**, *23*, 4810.
(19) Sels, B.; Vos, D. D.; Buntinx, M.; Pierard, F.; Mesmaeker, K. D.; Jacobs, P. *Nature* **1999**, *400*, 855.
(20) Zhou, C. H.; Beltramini, J. N.; Lin, C. X.; Xu, Z. P.; Lu, G. Q.; Tanksale, A. *Catal. Sci. Technol.* **2011**, *1*, 111.
(21) Choudary, B. M.; Madhi, S.; Chowdari, N. S.; Kantam, M. L.; Sreedhar, B. *J. Am. Chem. Soc.* **2002**, *124*, 14127.
(22) Gunjakar, J. L.; Kim, T. W.; Kim, H. N.; Kim, I. Y.; Hwang, S. J. *J. Am. Chem. Soc.* **2011**, *133*, 14998.
(23) Gu, Z.; Thomas, A. C.; Xu, Z. P.; Campbell, J. H.; Lu, G. Q. *Chem. Mater.* **2008**, *20*, 3715.
(24) Shao, M. F.; Wei, M.; Evans, D. G.; Duan, X. *Chem. Commun.* **2011**, *47*, 3171.
(25) Yan, D. P.; Lu, J.; Wei, M.; Qin, S. H.; Chen, L.; Zhang, S. T.; Evans, D. G.; Duan, X. *Adv. Funct. Mater.* **2011**, *21*, 2497.
(26) Han, J. B.; Dou, Y. B.; Wei, M.; Evans, D. G.; Duan, X. *Angew. Chem., Int. Ed.* **2010**, *49*, 2171.
(27) Shao, M. F.; Han, J. B.; Shi, W. Y.; Wei, M.; Duan, X. *Electrochem. Commun.* **2010**, *12*, 1077.
(28) Woo, M. A.; Song, M. S.; Kim, T. W.; Kim, I. Y.; Ju, J. Y.; Lee, Y. S.; Kim, S. J.; Choy, J. H.; Hwang, S. J. *J. Mater. Chem.* **2011**, *21*, 4286.
(29) Wang, L.; Wang, D.; Dong, X. Y.; Zhang, Z. J.; Pei, X. F.; Chen, X. J.; Chen, B.; Jin, J. *Chem. Commun.* **2011**, *47*, 3556.
(30) Gao, Z.; Wang, J.; Li, Z.; Yang, W.; Wang, B.; Hou, M.; He, Y.; Liu, Q.; Mann, T.; Yang, P.; Zhang, M.; Liu, L. *Chem. Mater.* **2011**, *23*, 3509.
(31) Géraud, E.; Rafqah, S.; Sarakha, M.; Forano, C.; Prevot, V.; Leroux, F. *Chem. Mater.* **2008**, *20*, 1116.
(32) Hsu, W. P.; Yu, R.; Matijevic, E. *J. Colloid Interface Sci.* **1993**, *156*, 56.
(33) Zhao, Y. F.; He, S.; Wei, M.; Evans, D. G.; Duan, X. *Chem. Commun.* **2010**, *46*, 3031.
(34) Yu, J.; Yu, J. C.; Leung, M. K.-P.; Ho, W.; Cheng, B.; Zhao, X. J.; Zhao, J. C. *J. Catal.* **2003**, *217*, 69.
(35) Sing, K. S. W.; Everett, D. H.; Haul, R. A. W.; Moscou, L.; Pierotti, R. A.; Rouquerol, J.; Siemieniewska, T. *Pure Appl. Chem.* **1985**, *57*, 603.
(36) Futaba, D. N.; Hata, K.; Yamada, T.; Hiraoka, T.; Hayamizu, Y.; Kakudate, Y.; Tanaike, O.; Hatori, H.; Yumura, M.; Iijima, S. *Nat. Mater.* **2006**, *5*, 987.
(37) Zhou, H.; Li, D.; Hibino, M.; Honma, I. *Angew. Chem., Int. Ed.* **2005**, *44*, 797.
(38) Yang, G.; Xu, C.; Li, H. *Chem. Commun.* **2008**, *44*, 6537.

(39) Jiang, H.; Zhao, T.; Li, C. Z.; Ma, J. *J. Mater. Chem.* **2011**, *21*, 3818.
(40) Zang, J. F.; Bao, S. J.; Li, C. M.; Bian, H. J.; Cui, X. Q.; Bao, Q. L.; Sun, C. Q.; Guo, J.; Lian, K. R. *J. Phys. Chem. C* **2008**, *112*, 14843.
(41) Fabio, A. D.; Giorgi, A.; Mastragostino, M.; Soavi, F. *J. Electrochem. Soc.* **2001**, *148*, A845.
(42) Kotz, R.; Carlen, M. *Electrochim. Acta* **2000**, *45*, 2483.
(43) Liu, J.; Cheng, C.; Zhou, W.; Lia, H.; Fan, H. J. *Chem. Commun.* **2011**, *47*, 3436.